Proceedings of the 20th International Conference on Soil Mechanics and Geotechnical Engineering– Rahman and Jaksa (Eds)

A coupled computational framework for modelling fluid pressurised crack evolution in porous media

Un cadre de calcul entièrement couplé pour l'évolution des fissures sous pression de fluide dans les milieux poreux

Mohaddeseh Mousavi Nezhad & Nima Sarmadi
School of Engineering, University of Warwick, UK, m.mousavi-nezhad@warwick.ac.uk

ABSTRACT: This paper presents a computational framework for modelling hydraulic fracture on the basis of the saturated porous continuum concept and phase-field theory. By considering the continuum as two damaged and intact domains, model components are isolated and considered separately, simplifying the whole modelling approach. Mathematical models are derived based on the energy minimisation of the fracturing continuum space governing the mechanical deformation and damage evolution as well as the compressible fluid flow through the damaged and intact porous media. We particularly focus on the flow of fluid within the intact and damaged porous zones. The exchange of the fluid between damaged and intact zones is governed by the evolution of the permeability due to porosity change and the formed crack-width over the continuum domain. The evolution of the crack is modelled using Francfort and Marigo's variational approach, which approximates the fracture by a diffusive damage zone using a phase-field variable. The method is benchmarked by analysing a number of examples which allow testing its performance in predicting hydraulically driven fracture process and the associated domain permeability variations.

RÉSUMÉ : Cet article présente un cadre de calcul pour la modélisation de la fracture hydraulique sur la base de la combinaison du continuum poreux saturé et de la théorie du champ de phase. En considérant le continuum comme deux domaines distincts de domaines endommagés et intacts, les composants du modèle sont isolés et considérés séparément, ce qui simplifie toute l'approche de modélisation. Le modèle mathématique est basé sur la minimisation d'énergie de l'espace continu de fracturation régissant la déformation mécanique et l'évolution des dommages ainsi que l'écoulement du fluide compressible dans les milieux poreux endommagés et intacts. Nous nous concentrons particulièrement sur l'écoulement du fluide dans les zones poreuses intactes et endommagées. L'échange de fluide entre les zones endommagées et intactes est régi par l'évolution de la perméabilité due au changement de porosité et la largeur de fissure formée sur le domaine continu. L'évolution des fissures est modélisée en utilisant l'approche variationnelle de Francfort et Marigo, qui se rapproche de la fracture par une zone d'endommagement diffusif à l'aide d'une variable de champ de phase. La méthode est vérifiée en analysant des exemples de référence, et la performance met en évidence ses capacités à prédire le processus de fracture hydraulique et les variations de perméabilité associées.

KEYWORDS: Hydraulic fracturing, porous media, geo-energy, phase-field crack modelling.

1 INTRODUCTION

Hydraulic fracturing is a hydromechanical process in which pressurised fluid is injected into the wellbore connected to the target subsurface layers to develop a fracture network throughout the porous medium. After the invention of this method, basic analytical solutions, such as PKN and KGD models, were introduced to the engineering community to predict the hydraulic fracture propagation and the changes of the inner-crack fluid pressure (Geertsma & De Klerk, 1969; Perkins & Kern, 1961).

The fluid-driven fractures are mainly induced in low permeable geotechnical formations such as shale hosting conventional reservoirs (Arthur et al., 2009) and granite formations to exploit geothermal energy (Glassley, 2013). The propagation of cracks in the porous medium includes pore space collapses and the coalescence of crack-like pores within the solid skeleton, which causes changes in the hydro-mechanical response of the medium (Detournay & Cheng, 1993). This process can be simplified into a mathematical model consisted of two dissipative process, the creation of new surfaces and the flow of a viscous fluid within the fracture network, which was in line with laboratory observations (Bunger & Detournay, 2008; Savitski & Detournay, 2002). The numerical methods are suitable for the simulation and prediction of the hydraulic fracturing process in the real-world practical works, where the complexities in both geometrical and hydro-mechanical properties of the geotechnical formations are inevitable. It is more convenient to include most of the variables in the problem such as the permeability and the porosity of the porous medium, the leak-off and flow-back regimes around the crack, and the mechanical rupture and deformations around the crack-tip, using numerical methods (Lecampion, Bunger, & Zhang, 2018). Various methods have been utilised to study the hydraulic fracture propagation in porous media, among which the finite element method shows a great performance in dealing with irregular crack topographies, heterogeneities, and the nonlinearities in the material.

In a thorough investigation of fracking in porous media, the fluid exchange between the fracture network and the intact solid skeleton is prominent in the prediction of inner-crack fluid pressure, the productivity of the wellbore in the stimulation of the conventional resources and in the extraction of geothermal energy. The fundamentals of the linear elastic fracture mechanics also contribute to the formulations by determining the direction of the crack propagation and the stress field. The extended finite element method is one the widely used methods in this field, which is capable of considering these complicated processes in fractured reservoirs (Vahab, Akhondzadeh, Khoei, & Khalili, 2018; Vahab & Khalili, 2017). Despite the robustness of this method in modelling hydraulic fracturing process, it somehow suffers from predicting the nucleation of the new cracks due to random weaknesses in the medium (Gironacci et al., 2018 and Mousavi Nezhad, et. al., 2018). In this regard, the phase-field approach (Bourdin, Francfort, & Marigo, 2000) is recognised as a versatile method in prediction of the direction and length of brittle cracks based on the energy representation of the crack introduced by Griffith. This method was gradually developed to

apply in modelling dynamic (Borden, et al., 2012) and ductile (Ambati, et al., 2015) fracturing, and fluid-driven fractures in poro-elastic media (Heider & Markert, 2017; Christian Miehe & Mauthe, 2016; Mikelić, et al., 2015; Wilson & Landis, 2016).

In this study, we introduce a mathematical framework to predict the hydraulic fracture propagation based on the phase-field theory (Francfort & Marigo, 1998) throughout porous media in the realm of large deformations and finite strains. The crack formation results in the appearance of the crack-width and the increase in porosity due to the large deformations within the damaged zone. Therefore, the mechanical properties and the hydraulic transmissivity change in accordance with the crack evolution. The proposed formulation is constructed from a crack evolution model based on the phase-field theory and a geometrically nonlinear fully coupled model to capture the hydromechanical behaviour of the porous medium. In this model, the hydraulic transmissivity evolves using Poiseuille's law for the cracked region and Kozney-Carman equation for the change of porosity in the porous matrix. A compressible Neo-Hookean constitutive model is considered to model the hyper-elastic mechanical behaviour of the solid skeleton which is coupled in a staggered manner with the damage state of the body using tensile and compressive energy functionals introduced by Miehe (Miehe et al., 2010). The verification and validation of the method is investigated by comparing the numerical results to the experimental findings in Cheng et al. (2020) on the propagation of hydraulic fracture and pressure changes in cubic samples of granite.

2 MATHEMATICAL FORMULATIONS

Hydraulic fracturing in porous media happens in a nonlinear manner due to the changes in compressibility of pore spaces and the stiffness of solid skeleton (Detournay & Cheng, 1993). The purpose of this study is to develop a framework capable of capturing the most prominent constitutive aspects in a geometrically nonlinear setting.

It is pointed out here that building the formulations upon the fundamentals of large deformations and finite strains requires defining the deformation function. The deformed body is recognized by spatial coordinates $\boldsymbol{x}_i$ and can be mapped over the reference undeformed configuration Ω_0 using $\boldsymbol{x} = \boldsymbol{\phi}(\boldsymbol{X}, t)$, where $\boldsymbol{X}_i$ are defined as material coordinates. Accordingly, the deformation gradient tensor is defined as

$$\boldsymbol{F}(\boldsymbol{X}, t) = \frac{\partial \boldsymbol{\phi}(\boldsymbol{X},t)}{\partial \boldsymbol{X}_i} = \nabla_{\boldsymbol{X}}(\boldsymbol{\phi}) \tag{1}$$

2.1 *The evolution of cracks in the porous medium*

A macroscopic approach to study the hydro-mechanical behavior of porous media is adopted based on Biot's theory (Biot & Temple, 1972), and the concept of effective stresses is introduced as

$$\boldsymbol{\sigma} = \boldsymbol{\sigma}' - \alpha p \boldsymbol{I} \tag{2}$$

where, $\boldsymbol{\sigma}$ is the total Cauchy stress tensor defined on the reference deformed configuration, $\boldsymbol{\sigma}'$ is the effective stress tensor, α is the Biot's coefficient, and $p\boldsymbol{I}$ is the hydrostatic fluid pressure tensor. Since the bulk modulus (K) of soil mass is negligible compared to that of solid grains, α can be assumed as equal to unity. Conversely, the drained bulk modulus of rock mass is significantly large so that the Biot coefficient α should be measured for the rocks in laboratory (Franquet & Abass, 1999). The following relationship is used for α depending on drained bulk and solid phase bulk moduli (K, K_s).

$$\alpha = 1 - K/K_s \tag{3}$$

When the porous medium is subjected to hydraulic and mechanical loading, the free bulk energy of the body increases, and it is energetically favourable for the system to release energy by forming new surfaces over the volume (Mousavi Nezhad et al., 2018). Having adopted the phase-field theory to model the hydraulic fracture propagation, the whole modelling process is reduced to the minimization of the total energy of the system with respect to the variables. The internal potential energy of the system is formed in the following as a functional of displacement field $\boldsymbol{u}$, the fluid pressure p, and the damage state in the medium s over the reference volume Ω_0, which is called $\mathbb{W}(\boldsymbol{u}, p, s)$.

$$\mathbb{W} = \int_{\Omega_0}\left((s^2 + \kappa_\varepsilon)\Psi^+_{\text{eff}}(\boldsymbol{C}) + \Psi^-_{\text{eff}}(\boldsymbol{C})\right)dV + \int_{\Omega_0}\Psi_{\text{fluid}}(J, p)dV + \frac{G_c}{2}\int_{\Omega_0}\left(\varepsilon\|\nabla_{\boldsymbol{X}}(s)\|^2 + \frac{1}{\varepsilon}(1-s)^2\right)dV \tag{4}$$

In this functional, the effective energy of the solid skeleton is degraded due to the evolution of damage zone within the volume, following the energy split by (Miehe & Mauthe, 2016), the fluid energy depends on volumetric deformation and the amount of fluid flowing into the medium, and the last integral represents the amount of surface energy developed in the body (Bourdin et al., 2000). The effective energy is dependent on the deformation and is written in terms of the right Cauchy-Green deformation tensor $\boldsymbol{C} = \boldsymbol{F}^T \cdot \boldsymbol{F}$, whereas the fluid energy is dependent on the fluid pressure and the volumetric strain $(J-1)$, where $J = \det(\boldsymbol{F})$. The concept of effective stress is pushed back over the reference configuration using two energetically conjugate quantities, the second Piola-Kirchhoff effective stress tensor $\boldsymbol{S}'$ and the Green-Lagrange strain $\boldsymbol{E}$ as

$$\boldsymbol{S} = \boldsymbol{S}' - \alpha(Jp)\boldsymbol{C}^{-1} \tag{5}$$

$$\boldsymbol{E} = \frac{1}{2}(\boldsymbol{C} - \boldsymbol{I}) \tag{6}$$

where, $\boldsymbol{S}' = \boldsymbol{F}^{-1} \cdot J\boldsymbol{\sigma}' \cdot \boldsymbol{F}^{-T}$. The finite element weak form of the crack evolution model is reached by minimising the energy function with respect to the arbitrary damage variable ψ as

$$\int_{\Omega_0} 2\Psi^+_{\text{eff}}(\boldsymbol{C})\, s \cdot \psi d\text{V} + 2l_0 G_c \int_{\Omega_0} \nabla_{\boldsymbol{X}}(\psi) \cdot \nabla_{\boldsymbol{X}}(s) d\text{V} - \frac{G_c}{2l_0}\int_{\Omega_0}(1-s)\cdot\psi d\text{V} - 2l_0 G_c \int_{\partial\Omega_0}\psi\, \nabla_{\boldsymbol{X}}(s)\cdot\boldsymbol{N} dA = 0 \tag{7}$$

where, $\nabla_{\boldsymbol{X}}$ is the gradient operator with respect to the reference coordinates, G_c is the critical energy release rate of the material, and l_0 is the length-scale parameter representing the half-width of the smeared damaged zone. According to linear elastic fracture mechanics, the relationship between the tensile strength of the material and model parameters (Wilson & Landis, 2016) holds as

$$\sigma_{\text{tensile}} = \sqrt{EG_c/l_0} \tag{8}$$

where, E is Young's modulus of the material. The crack evolution model is coupled with the hydro-mechanical model using a staggered numerical approach, in a sense that the state of damage is kept fixed ($\bar{s}$) while solving for the $\boldsymbol{u}$-p problem. To govern the nonlinear hydro-mechanical behaviour of the porous medium, the Galerkin weak form of the mass conservation law is coupled monolithically with the principle of virtual work. By finding a stationary position of the energy functional $\mathbb{W}$ with respect to arbitrary displacements $\boldsymbol{\eta}$, the principle of virtual work reads

$$\int_{\Omega_0}(\bar{s}^2 + \kappa_\varepsilon)[\boldsymbol{S}']^+ : D\boldsymbol{E}[\boldsymbol{\eta}]dV + \int_{\Omega_0}[\boldsymbol{S}']^- : D\boldsymbol{E}[\boldsymbol{\eta}]dV - \int_{\Omega_0}(\alpha\theta)\boldsymbol{F}^{-1}\cdot\nabla_{\boldsymbol{X}}\cdot\boldsymbol{\eta}\, d\text{V} - \delta W_{\text{ext}} = 0 \tag{9}$$

where, $\theta = Jp$ is the Kirchhoff fluid pressure and the effective stress tensor is obtained via $\boldsymbol{S}' = 2\,\Psi_{\text{eff}}(\boldsymbol{C})/\partial\boldsymbol{C}$, where a compressible Neo-Hookean hyper-elastic model is used to model the behavior of the solid skeleton as

$$\Psi_{\text{eff}}(\boldsymbol{C}) = \frac{1}{2}\lambda(\ln J)^2 - \mu \ln J + \frac{1}{2}\mu(\text{tr}(\boldsymbol{C}) - 3) \quad (10)$$

where, λ and μ are elastic Lame parameters.

2.2 *The fluid flow in the fractured porous mixture*

The mass conservation law coupled with Darcy's law to govern the fluid flow throughout the porous system is denoted in the following form.

$$\alpha\dot{J} + \dot{p}/M + J\boldsymbol{F}^{-1} \cdot \nabla_{\boldsymbol{X}} \cdot (\boldsymbol{v}^r) = 0 \quad (11)$$

$$\boldsymbol{v}^r = -\left(\bar{\boldsymbol{k}}/\mu_{\text{f}}\right)(\boldsymbol{F}^{-1} \cdot \nabla_{\boldsymbol{X}}(p) - \rho_{\text{f}}\boldsymbol{G}) \quad (12)$$

where, $\bar{\boldsymbol{k}}$ is the intrinsic permeability tensor, μ_{f} is the fluid viscosity, M is Biot's modulus of the porous mixture, and $\boldsymbol{v}^r$ is the well-known relative Darcy velocity defined in the spatial form over the current surface boundary of the body. The propagation of the hydraulic fracture within the domain results in the appearance of a discontinuous displacement field around the crack, which is recognised as the crack width w. The fluid flow regime inside the fully damaged zone is better governed by Poiseuille's law (Miehe & Mauthe, 2016) defined in the Eq. (13). Also, the crack propagation and the evolution of deformation causes significant changes in pore spaces. The evolution of porosity mostly affects the fluid pressure distribution throughout the domain, and such deformation-induced behaviour is captured by including the Kozney-Carman relationship, Eq. (14), to modify the permeability tensor in the step-by-step nonlinear analysis (Choo, 2018).

$$\boldsymbol{v}^r = -(w^2/\mu_{\text{f}})\boldsymbol{F}^{-1} \cdot \nabla_{\boldsymbol{X}}(p) \quad (13)$$

$$\boldsymbol{k}_{n+1} = \boldsymbol{k}_n(\varphi_{n+1}^3/\varphi_n^3)((1-\varphi_n^2)/(1-\varphi_{n+1}^2)) \quad (14)$$

The evolution of the porosity (φ) in the medium in n-th step can be calculated using

$$\varphi_n = 1 - (1-\varphi_0)/J_n \quad (15)$$

where, φ_0 is the initial value of porosity in the undeformed body, and J_n is the Jacobian of deformation in n-th step.

3 NUMERICAL SIMULATIONS

The verification of the method is done in two steps; first, the hydro-mechanical model is verified; second, the whole hydraulic fracture model is tested using experimental data.

3.1 *one-dimensional consolidation problem*

The nonlinear hydro-mechanical model is verified by simulating the one-dimensional consolidation problem of a soil material provided in Borja, et al. (1998). An extra pressure load of 90kPa is applied over the soil column instantly. The nonlinear finite strain model is capable of predicting the large settlement in the soil column, whereas the small strain theory based on Terzaghi's analytical solution does not consider the geometrical large deformations. The numerical results shown in the Fig. 1 match well with the findings of Borja et al. (1998) and is compared to the analytical solution of Terzaghi. The excess pore pressure dissipation is depicted in Fig. 2 using isochrones in subsequent snapshots from the beginning to the end of process. The results are promising and are in good agreement with the study (Borja et al., 1998), which shows the reliability of the model to host the hydraulic fracture propagation model.

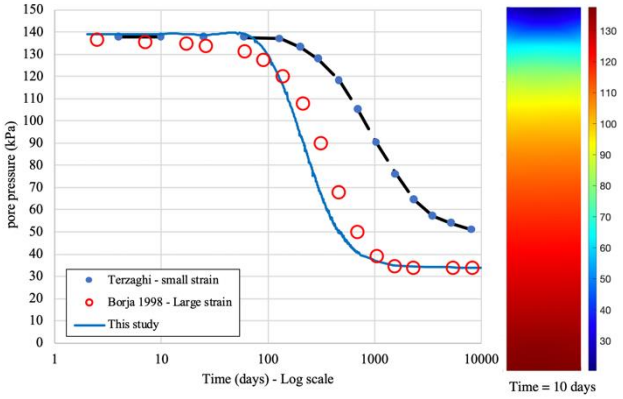

Figure 1. The pore pressure dissipation of the bottom of the soil column in time. The comparison between our findings and (Borja et al., 1998).

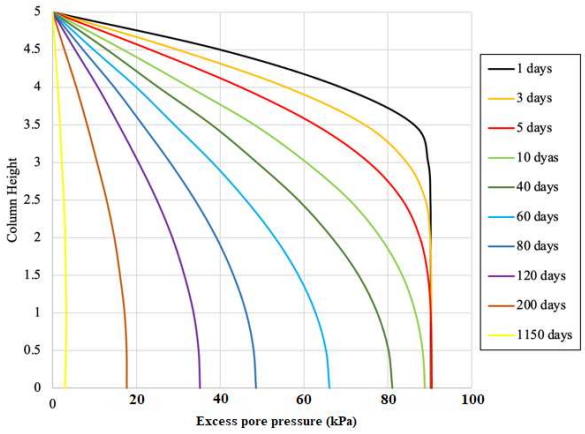

Figure 2. The pore pressure isochrones of the process of consolidation.

3.2 *Hydraulic fracturing in granite*

The hydraulic fracture propagation model in this study is verified by simulating the boundary value problem as defined in the work by Cheng et al. (2020) to induce fluid-driven fracture in a plane strain domain of granite material, as shown in Fig. 3. The material properties to run the simulations are listed in Table 1.

Table 1. Material properties to simulate hydraulic fracturing.

Parameter (unit)	*Value*
Young's modulus E (GPa)	39.99
Poisson's ratio	0.28
Porosity φ_0	0.0322
Brazilian tensile strength (MPa)	18.54
Length-scale parameter l_0	0.002
Intrinsic Permeability (millidarcy)	0.034
Critical energy release rate (N/m)	40

The far-field stress σ_1 and σ_2 are applied in horizontal and vertical directions respectively. Different injection rates 5, 10, 15, and 20mL/min are chosen to pump the fluid into the granite sample. Three combinations of far-field stresses (σ_1, σ_2) in MPa are set on the boundaries as (4,6), (8,12), and (12,18). The fluid injection pressure into the middle wellbore, the crack width,

and the breakdown pressure are chosen to be investigated in the numerical simulations.

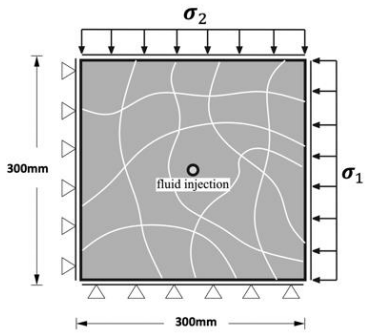

Figure 3. The boundary value problem to drive hydraulic fracture in the granite specimen as defined by (Cheng et al., 2020).

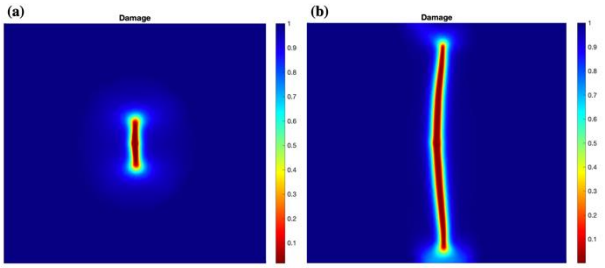

Figure 4. The crack pattern for the case of injection rate 10mL/min and $\sigma_1 = 4MPa$ and $\sigma_2 = 6MPa$. (a) is after breakdown, (b) is before rupturing the specimen.

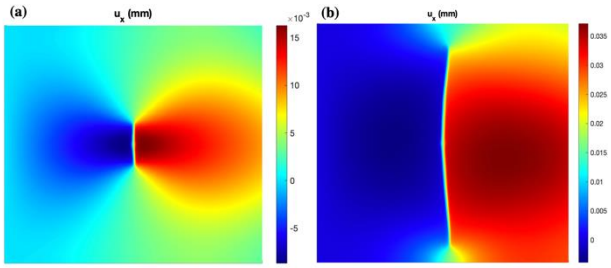

Figure 5. The displacement field around the crack for the case of injection rate 10mL/min and $\sigma_1 = 4MPa$ and $\sigma_2 = 6MPa$. (a) is after breakdown, (b) is before rupturing the specimen.

The crack pattern, as shown in Fig. 4, shows that the crack has propagated in the direction of the maximum far-field stresses applied as expected. The displacement field is shown in the Fig. 5 to illustrate the capability of the phase-field approach to capture the discontinuity in the displacement field on the same continuous finite element mesh. Fig. 6 shows the distribution of the fluid pressure in the medium. The majority of the fluid flow happens inside the crack, and the pressure gradient is focused around the tips, where the leak-off into the intact porous matrix is observed. A concentration around the well-bore is captured in the simulations, whereas a uniform fluid pressure inside the crack is reached due to the high permeability.

Fig. 7 shows the changes of the injection pressure inside the wellbore and compares the findings for two cases of the injection rates of 5mL/min and 20mL/min and the far-field stresses of $\sigma_1 = 8MPa$ and $\sigma_1 = 12MPa$ in this study to the experimental results provided by Cheng et al. (2020). In the experimental data, a build up of fluid pressure is seen with an increasing slope at the beginning of the injection, which is not the case for the numerical results because the medium is already considered to be fully saturated. In these curves, the injection pressure increases as the fluid in being pumped into the well and reaches to a steep drop point, called "breakdown pressure", which is the start of the fracture propagation. A nice agreement can be seen between the predicted results of the phase-field hydraulic fracture model with the experiments addressed in Cheng et al. (2020). Also, the increase of the injection rate causes a considerable amount of increase in the breakdown fluid pressure which is in line with the experimental observations. According to both numerical and experimental results, the fluid injection rate into the wellbore is influential in timing of the process, causing the fracture to propagate slower, which is evident by comparing two cases of injection rate in Fig. 7. By the propagation of the hydraulic fracture from the tips toward the edges of the specimen, the inner-crack pressure keeps decreasing due to the simultaneous increase of the volumetric strain and porosity. As shown in the Fig. 7, this numerical framework is capable of not only predicting the breakdown pressure but also capturing the gradual drop in the pressure due to the evolution of porosity, compatible with the experimental findings in Cheng et al. (2020).

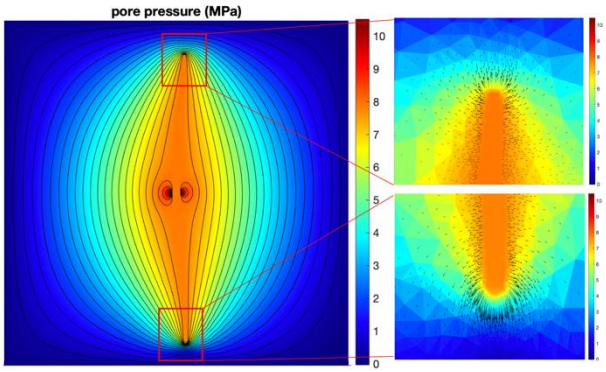

Figure 6. The distribution of the fluid pressure inside the crack and the porous medium. The magnified snapshots on the right shows the leak-off from the crack-tip into the intact porous medium, neglecting the main flow channel inside the cracked zone.

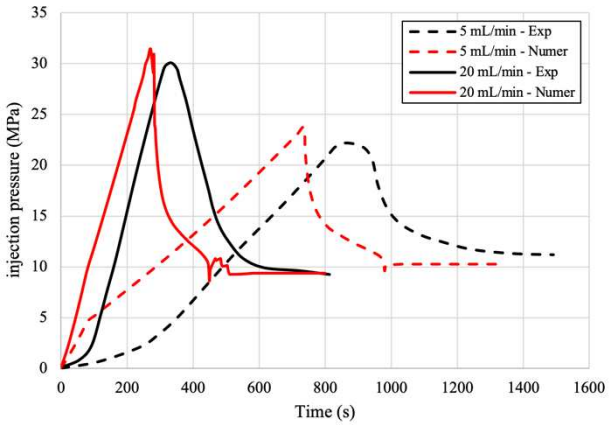

Figure 7. The comparison between our numerical results of the injection fluid pressure and experimental findings in (Cheng et al., 2020) for two fluid injection rates while far-field stresses are 8MPa and 12MPa.

According to the experimental observations, the fluid injection pressure becomes constant after rupturing the specimen, when one of the tips touches the outer boundary. After the completion of the hydraulic fracturing process, the injection pressure remains constant if the same fluid injection rate is still pumped into the wellbore. The reason behind this behaviour can be interpreted such that a minimum amount of the inner-crack fluid pressure is required to keep the crack open and to keep the fluid flowing out of the domain. The time histories of the hydraulic fracture opening for different cases of the fluid

injection point is shown in Fig. 8 for the case of far-field stresses $\sigma_1 = 4MPa$ and $\sigma_1 = 6MPa$. It is evident that by reaching to the breakdown pressure, the opening increases suddenly, meaning that the initial crack has been formed. By the propagation of the fracture, the crack-width keeps increasing until reaching to its peak value, which is indeed before the stage of touching the outer boundary. The graphical situation of this stage is shown in Fig. 5. The crack propagation stops afterwards, and the hydraulic fracture experiences a closure which is seen in the sudden drop of the crack-width time histories in Fig. 8. The increase of the injection rate causes the maximum value of the crack-width increase, which can be interpreted with regards to the injection pressure in a sense that the higher injection rate generates higher pressure causing larger opening.

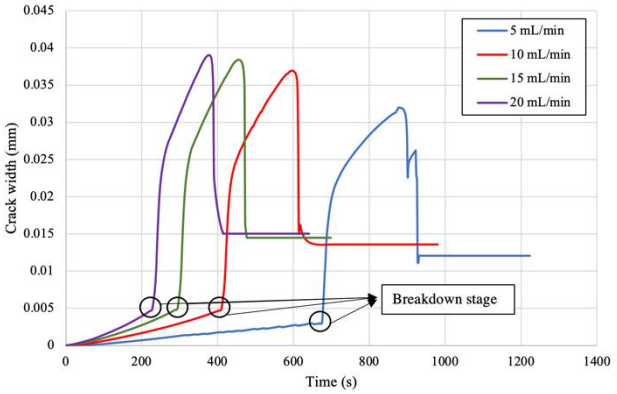

Figure 8. Time histories for crack-width in the process of hydraulic fracturing for different values of the fluid injection rate.

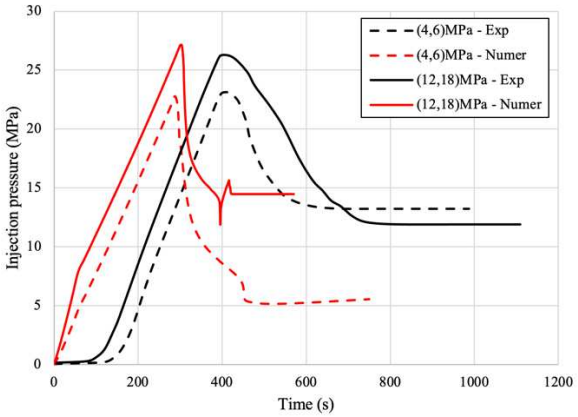

Figure 9. The comparison between numerical results of the injection pressure evolution and experimental data in Cheng et al. (2020). regarding the effect of far-field stresses.

The effect of far-field stresses on the process of hydraulic fracturing can be investigated considering Fig. 9. According to the experimental observations of Cheng et al. (2020), the increase of far-field stresses causes results in the requirement of a higher injection fluid pressure into the wellbore to start the breakdown stage. Considering the same injection rate, the slope of the curves reaching to the breakdown pressure are the same. However, the experiments are done in an unsaturated condition so that a lag is seen between numerical and experimental results. According to Fig. 9, the numerical model seems to be capable enough to predict the effect of the increase of far-field stresses on the breakdown pressure. This conclusion is in accordance to the experimental data; however, the predicted value for the required injection pressure after the completion of the hydraulic fracture propagation seems to be different from the experimental results. After the completion of the crack propagation, the far-field stresses act in the way of reducing the openness of the crack. As a result, by the increase of these external loads, the required fluid pressure is found to be increased in the numerical results. This steady fluid pressure in the experiments has been found to be decreased by the increase of the far-field stresses. The numerical results imply that the increase of the far-field stresses is influential on the total timing of the process such that the increase of far-field stresses has resulted in a faster crack propagation by having the same fluid injection rate. It is worth mentioning that the experiments conducted in Cheng et al. (2020) were influenced by heat, which has not been considered in this study, and the other conditions applied might have been different from the defined boundary conditions in our numerical simulations.

4 CONCLUSIONS

The proposed numerical model to simulate the process of hydraulic fracturing in compressible porous media is found to be capable of predicting the most prominent features of this technique and can be used in practical engineering applications. This framework is built upon the updated Lagrangian finite element formulation by coupling a phase-field fracture model with a nonlinear hydro-mechanical model at finite strains.

The phase-field crack which is implemented on a continuous finite element mesh is capable of modelling the fluid flow inside the crack channel as well as the leak-off into the intact porous solid using the general equation of the conservation of mass. Two techniques are implemented to consider the evolution of the permeability over the finite element mesh due to the pore collapses and cracking in the porous medium.

The most important findings of this study are listed below.

- Consideration of the large deformation theory and hyper-elastic materials is vital to consider the changes of the solid skeleton stiffness and porosity evolution in the nonlinear finite element analysis.
- Comparing the numerical results to experimental data, the theories considered to evolve the permeability based on the volumetric strains and to degrade the stiffness due to the development of damages work perfectly in predicting the breakdown fluid pressure, the crack propagation, and the effects of far-field stresses and injection rates.
- The fluid injection rate imposed on the wellbore is important in practical applications. Based on the results, the increase in the injection rate results in the increase of the breakdown pressure and the crack opening, although it has no effect on the steady pressure to keep the crack open after the completion of the process.
- Time histories of the injection pressure with respect to time, the hydraulic fracturing process is accelerated by increasing the injection rate and the far-field stresses.
- The direction of the maximum far-field stresses specifies the direction of the hydraulic fracture propagation without using any further criteria, which is not possible readily in other methods.
- The increase in the far-field stresses requires a greater breakdown pressure inside the wellbore to initiate the propagation. It is also found that the fluid pressure inside the crack after the completion of the propagation, needed to keep the crack opened, increases when larger far-field stresses applies to the system.

Since this framework is implemented on a continuous finite element mesh and rests on the minimisation of the system energy, it can be extended to model the spatial heterogeneities of underground reservoirs in a computational efficient manner.

5 REFERENCES

Ambati, M., Gerasimov, T., & De Lorenzis, L. (2015). Phase-field modeling of ductile fracture. Computational Mechanics, 55(5), 1017-1040. doi:10.1007/s00466-015-1151-4

Arthur, J. D., Bohm, B. K., Coughlin, B. J., Layne, M. A., & Cornue, D. (2009). Evaluating the Environmental Implications of Hydraulic Fracturing in Shale Gas Reservoirs. Paper presented at the SPE Americas E&P Environmental and Safety Conference.

Biot, M. A., & Temple, G. (1972). Theory of finite deformations of porous solids. Indiana University Mathematics Journal, 21(7), 597-620.

Borden, M. J., Verhoosel, C. V., Scott, M. A., Hughes, T. J. R., & Landis, C. M. (2012). A phase-field description of dynamic brittle fracture. Computer Methods in Applied Mechanics and Engineering, 217-220, 77-95. doi:https://doi.org/10.1016/j.cma.2012.01.008

Borja, R. I., Tamagnini, C., & Alarcón, E. (1998). Elastoplastic consolidation at finite strain part 2: finite element implementation and numerical examples. Computer Methods in Applied Mechanics and Engineering, 159(1), 103-122. doi:https://doi.org/10.1016/S0045-7825(98)80105-9

Bourdin, B., Francfort, G. A., & Marigo, J. J. (2000). Numerical experiments in revisited brittle fracture. Journal of the Mechanics and Physics of Solids, 48(4), 797-826. doi:https://doi.org/10.1016/S0022-5096(99)00028-9

Bunger, A. P., & Detournay, E. (2008). Experimental validation of the tip asymptotics for a fluid-driven crack. Journal of the Mechanics and Physics of Solids, 56(11), 3101-3115. doi:https://doi.org/10.1016/j.jmps.2008.08.006

Cheng, Y., Zhang, Y., Yu, Z., Hu, Z., & Yang, Y. (2020). An investigation on hydraulic fracturing characteristics in granite geothermal reservoir. Engineering Fracture Mechanics, 237, 107252. doi:https://doi.org/10.1016/j.engfracmech.2020.107252

Choo, J. (2018). Large deformation poromechanics with local mass conservation: An enriched Galerkin finite element framework. International Journal for Numerical Methods in Engineering, 116(1), 66-90. doi:10.1002/nme.5915

Detournay, E., & Cheng, A. H. D. (1993). 5 - Fundamentals of Poroelasticity. In C. Fairhurst (Ed.), Analysis and Design Methods (pp. 113-171). Oxford: Pergamon.

Francfort, G. A., & Marigo, J. J. (1998). Revisiting brittle fracture as an energy minimization problem. Journal of the Mechanics and Physics of Solids, 46(8), 1319-1342. doi:https://doi.org/10.1016/S0022-5096(98)00034-9.

Franquet, J. A., & Abass, H. H. (1999). Experimental evaluation of Biot's poroelastic parameterThree different methods. Paper presented at the Vail Rocks 1999, The 37th U.S. Symposium on Rock Mechanics (USRMS).

Geertsma, J., & De Klerk, F. (1969). A Rapid Method of Predicting Width and Extent of Hydraulically Induced Fractures. Journal of Petroleum Technology, 21(12), 1571-1581. doi:10.2118/2458-pa

Gironacci, E. Mousavi Nezhad, M., Rezania, M. and Lancioni, G. (2018). A non-local probabilistic method for modeling of crack propagation. International Journal of Mechanical Sciences, 144, 897-908.

Glassley, W. E. (2013). Geothermal Energygeothermalenergy, Geologygeothermalenergygeologyand Hydrologygeothermalenergyhydrologyof. In M. Kaltschmitt, N. J. Themelis, L. Y. Bronicki, L. Söder, & L. A. Vega (Eds.), Renewable Energy Systems (pp. 761-771). New York, NY: Springer New York.

Heider, Y., & Markert, B. (2017). A phase-field modeling approach of hydraulic fracture in saturated porous media. Mechanics Research Communications, 80, 38-46. doi:https://doi.org/10.1016/j.mechrescom.2016.07.002

Lecampion, B., Bunger, A., & Zhang, X. (2018). Numerical methods for hydraulic fracture propagation: A review of recent trends. Journal of Natural Gas Science and Engineering, 49, 66-83. doi:https://doi.org/10.1016/j.jngse.2017.10.012

Miehe, C., & Mauthe, S. (2016). Phase field modeling of fracture in multi-physics problems. Part III. Crack driving forces in hydro-poro-elasticity and hydraulic fracturing of fluid-saturated porous media. Computer Methods in Applied Mechanics and Engineering, 304, 619-655. doi:https://doi.org/10.1016/j.cma.2015.09.021

Miehe, C., Welschinger, F., & Hofacker, M. (2010). Thermodynamically consistent phase-field models of fracture: Variational principles and multi-field FE implementations. International Journal for Numerical Methods in Engineering, 83(10), 1273-1311. doi:10.1002/nme.2861

Mikelić, A., Wheeler, M. F., & Wick, T. (2015). A Phase-Field Method for Propagating Fluid-Filled Fractures Coupled to a Surrounding Porous Medium. Multiscale Modeling & Simulation, 13(1), 367-398. doi:10.1137/140967118

Mousavi Nezhad, M., Fisher, Q. J., Gironacci, E., & Rezania, M. (2018). Experimental Study and Numerical Modeling of Fracture Propagation in Shale Rocks During Brazilian Disk Test. Rock Mechanics and Rock Engineering, 51(6), 1755-1775. doi:10.1007/s00603-018-1429-x

Mousavi Nezhad, M., Gironacci, E., Rezania, M., & Khalili, N. (2018). Stochastic modelling of crack propagation in materials with random properties using isometric mapping for dimensionality reduction of nonlinear data sets. International Journal for Numerical Methods in Engineering, 113(4), 656-680. doi:10.1002/nme.5630

Perkins, T. K., & Kern, L. R. (1961). Widths of Hydraulic Fractures. Journal of Petroleum Technology, 13(09), 937-949. doi:10.2118/89-pa

Savitski, A. A., & Detournay, E. (2002). Propagation of a penny-shaped fluid-driven fracture in an impermeable rock: asymptotic solutions. International Journal of Solids and Structures, 39(26), 6311-6337. doi:https://doi.org/10.1016/S0020-7683(02)00492-4

Vahab, M., & Khalili, N. (2017). Numerical investigation of the flow regimes through hydraulic fractures using the X-FEM technique. Engineering Fracture Mechanics, 169, 146-162. doi:https://doi.org/10.1016/j.engfracmech.2016.11.017

Vahab, M., Akhondzadeh, S., Khoei, A. R., & Khalili, N. (2018). An X-FEM investigation of hydro-fracture evolution in naturally-layered domains. Engineering Fracture Mechanics, 191, 187-204. doi:10.1016/j.engfracmech.2018.01.025

Wilson, Z. A., & Landis, C. M. (2016). Phase-field modeling of hydraulic fracture. Journal of the Mechanics and Physics of Solids, 96, 264-290. doi:https://doi.org/10.1016/j.jmps.2016.07.019